INTERVAL ATTENUATION ESTIMATION

Hafiz J. Alshammery and M. Nafi Toksöz

Earth Resources Laboratory
Department of Earth, Atmospheric, and Planetary Sciences
Massachusetts Institute of Technology
Cambridge, MA 02139

ABSTRACT

The goal of this paper is to study the accuracy of estimating the Quality Factor (Q) from ultrasonic pre-stack P-wave reflection data. Q is estimated by applying the spectral ratio method to the top and bottom reflections of the target. The data used to estimate Q are shot gathers acquired over different target materials submerged in a water tank. Using this setup, Q is estimated for Lucite, rubber and Berea sandstone. The behavior of Q estimates with offset is also investigated. Theoretical error analysis shows that non-zero estimates are contaminated by the overburden (water) attenuation. It is predicted that this error is directly proportional to the ratio of target depth to its thickness, target Q value, overburden attenuation and the difference between the top and bottom reflection ray trajectories in the overburden. The estimation error for Lucite is around 20%. For the Sandstone the error is about 10%. The estimated rubber Q is between 17 and 20. The estimates of all the targets show increasing estimated Q with increasing offset. This behavior is correctly predicted in the error analysis and is due to the difference between the top and bottom reflection ray path lengths within the overburden and the target Q value.

INTRODUCTION

Estimation of seismic wave attenuation is of practical importance due to the relation between attenuation and reservoir transport properties (Akbar *et al.*, 1994; Dvorkin *et al.*, 1994). Akbar *et al.* (1993) proposed that P-wave attenuation along the direction of maximum permeability is lower than attenuation along the direction of minimum permeability. So, attenuation measurements in multi-azimuth 3-D P-wave data may reveal permeability anisotropy in a fractured reservoir.

Many authors have attempted to estimate attenuation from different types of seismic

data. Liao and McMechan (1997) estimated Q using cross-well data. Stainsby and Worthington (1985) calculated attenuation from VSP data. Dasgupta and Clark (1994) estimated Q from CMP gathers. Jacobson (1987) investigated the relation between attenuation and velocity dispersion using refraction profiles.

In this study, Q is estimated from pre-stack P-wave data. Like most of the studies above, the spectral ratio method is used to compute attenuation. However, the estimation is performed for a single resolvable target zone using its top and bottom reflections observed at a given offset. This procedure eliminates the need for estimating the source signature; also, the interval attenuation calculated is closer to the true target Q value. The behavior of Q estimation with trace offset is investigated. Ultrasonic laboratory data sets are used in this study. Each data set represent a shot-gather acquired for a block of a target material submerged in a water tank.

DEFINITION OF Q

Q and its inverse are the most common measures of attenuation. Q is a dimensionless quantity which represents the ratio of the stored energy in a system to the dissipated energy. If the energy loss is small ($Q > 10$), then intrinsic Q may be defined as:

$$Q = -\frac{\omega E}{\frac{dE}{dt}} = -\frac{2\pi W}{\Delta W} \tag{1}$$

where E is the instantaneous energy of a system, dE/dt is the rate of energy loss, W is the stored elastic energy at maximum stress and strain and ΔW is the energy loss per cycle (Toksöz and Johnston, 1981). Relating Q to the amplitude (A) of an excitation rather than the elastic energy is more useful for data analysis. For linear wave propagation:

$$\begin{aligned} & W \propto A^2 \\ \text{Then:} \quad & \Delta W \propto 2A\Delta A \\ \text{and} \quad & Q = -\frac{\pi A}{\Delta A} \end{aligned} \tag{2}$$

where ΔA is the amplitude loss per cycle. In the case of 1-D propagation, ΔA can be expressed in terms of the wave length (λ) and the amplitude change per length as:

$$\Delta A = \lambda \frac{dA}{dx}.$$

Replacing λ by $\frac{2\pi c}{\omega}$, where c is the phase velocity and w is the angular frequency of the excitation, yields:

$$\Delta A = \frac{2\pi c}{\omega}\frac{dA}{dx}. \tag{3}$$

Substituting (3) in (2) and rearranging the equation relates the change in wave amplitude to Q and propagation distance (x) as:

$$\frac{1}{A}dA = -\frac{\omega}{2cQ}dx. \tag{4}$$

Equation (4) can be solved for the wave amplitude as a function of distance and frequency:

$$\begin{aligned} A(x,\omega) &= A(0,\omega)e^{-\frac{\omega}{2cQ}x} \\ &= A(0,\omega)e^{-\alpha x} \end{aligned} \tag{5}$$

where $A(0,\omega)$ is the initial amplitude spectrum of the wave and $\alpha = \left(\frac{\omega}{2cQ}\right)$ is defined as the attenuation coefficient of the medium (Baranowski, 1980). Equation (5) indicates that the amplitude of a propagating wave in an attenuating medium exhibits exponential decay behavior, with higher decay at high frequencies, and that $e^{-\alpha x}$ is the amplitude of the attenuation impulse response. Also, equation (5) is the basis for the spectral ratio method used to estimate Q of different materials.

SPECTRAL RATIO METHOD

The spectral ratio method is a widely used method to evaluate attenuation from seismic data. The spectral ratio method is based on taking the ratio of equation (5) at two positions x_1 and $x_2(x_1 < x_2)$. Ignoring body wave dispersion, the ratio x/c in (5) is replaced by the travel time (t) to point x. The logarithm of the spectral ratio is:

$$\ln\left|\frac{A(x_2,\omega)}{A(x_1,\omega)}\right| = -\frac{(t_2 - t_1)}{2Q}\omega = -s\omega \tag{6}$$

which is an equation of a straight line. To apply this method to data, one would estimate the slope of the ratio of the amplitude spectra recorded at times t_2 and t_1 with respect to frequency, then equate the absolute value of the slope to $(t_2 - t_1)/2Q$ and solve for Q. Equation (6) is also used to estimate Q from reflection data (White, 1992). In the 1-D convolutional model, an event $A(t)$ can be expressed as:

$$A(t) = s(t) * r(t) * q(t) * g(t) f_{\text{div}} \tag{7}$$

where $s(t)$ is the source wavelet, $r(t)$ is the reflectivity series, $q(t)$ is the attenuation impulse response, $g(t)$ is the receiver impulse response and f_{div} is the spherical divergence factor. Taking the ratio of (7) of two events $A(t1)$ and $A(t2)$ $(t1 < t2)$ in the frequency domain yields:

$$\left|\frac{A_2(\omega)}{A_1(\omega)}\right| = \left|\frac{R_2(\omega)f_{\text{div}}}{R_1(\omega)f_{\text{div}}}\right| e^{\frac{(t_2-t_1)}{2Q}\omega}.$$

If the reflectivity series is assumed to be white noise, the ratio of these series is frequency in dependent (Shatilo, 1994). The Logarithm of the previous expression is:

$$\ln\left|\frac{A_2(\omega)}{A_1(\omega)}\right| = \ln\left|\frac{R_2(\omega)f_{\text{div}}}{R_1(\omega)f_{\text{div}}}\right| + \frac{(t_2 - t_1)}{2Q}\omega. \tag{8}$$

Expression (8) represents the equation of a straight line, like (6), but with a non-zero intercept. However, the slope gives the Q information needed if the assumption about the reflectivity holds.

Q ESTIMATION ACCURACY

It has been observed that spectral ratio estimates of large Q values contain more error than estimates of smaller Q values. This error pattern is explained by the fact that as Q increases, the logarithm of the spectral ratio approaches a horizontal line. Estimating the slope of this line poses a numerical difficulty in the presence of noise (White, 1992). Estimates of very small Q values contain considerable error since the Q definition used in the spectral ratio method is valid for low loss materials ($Q > 10$). In addition to this type of error, the slope terms in equations (6) and (8) may be contaminated by propagation effects. In deriving (6) and (8), it is assumed that both waveforms share the same attenuation coefficient. However, when this method is used to calculated Q of a layer under some overburden, the overburden may not have the same Q value as the target and it is possible that the estimated target Q is influenced by the overburden attenuation.

To investigate the effect of overburden attenuation on the target Q estimate, consider the general earth model in Figure 1a. The model includes a layer stack with a source at the top and a receiver directly below the source at the bottom of the stack. Within each layer, only the intrinsic attenuation impulse response is considered. According to Bickel and Natarajan (1985), the attenuation impulse response is:

$$F(\omega) = e^{-ikx}$$

where $k = \beta - i\alpha$, x is the propagation distance, β is the wavenumber (ω/c) and α is the attenuation coefficient ($\omega/2cQ$). By expanding k, the impulse response becomes:

$$F(\omega) = e^{-\alpha x}e^{-i\beta x}.$$

The first exponential in this form is the amplitude decay factor, and the second exponential represents the propagation (phase) term. The recorded signal in Figure 1a, $R(t)$, is then the convolution of the source signal $S(t)$ with a cascaded system composed of the impulse responses of all the layers. In the frequency domain, the amplitude of the recorded signal is:

$$\begin{aligned} |R(\omega)| &= |S(\omega)||[|F_1(\omega)F_2(\omega)F_3(\omega)F_4(\omega)|] \\ &= |S(\omega)||[e^{-\alpha_1(x_1-x_0)}\ldots e^{-\alpha_4(x_4-x_3)}]. \end{aligned} \tag{9}$$

Interval Attenuation Estimation

To keep the math tractable, the top 3 layers in Figure 1a are replaced by a single attenuating layer, see Figure 1b. Using (9), the amplitudes of the top and bottom arrivals of the second layer, which is the target, are:

$$\begin{aligned} |R_1(\omega)| &= |S(\omega)|e^{-\alpha_1(x_1-x_0)} \\ |R_2(\omega)| &= |S(\omega)|[e^{-\alpha_1(x_1-x_0)}e^{-\alpha_2(x_2-x_1)}]. \end{aligned}$$

Normalizing the bottom amplitude spectrum by that of the top, the spectral ratio is:

$$|\frac{R_2(\omega)}{R_1(\omega)}| = e^{-\alpha_2(x_2-x_1)}. \tag{10}$$

The overburden operator canceled out by taking the spectral ratios; therefore, using equation (6) for estimating Q will not introduce overburden contamination for zero-offset traces.

For non-zero offset arrivals, the ray paths in the overburden will not coincide. The magnitude of the difference between the ray path lengths depends on the velocity distribution in and above the target. Using the ray geometry shown in Figure 1c, equation (10) becomes:

$$\left|\frac{R_2(\omega)}{R_1(\omega)}\right| = e^{-\alpha_2 l}e^{-\alpha_1\left(\frac{d}{\cos(t)}-\frac{d}{\cos(b)}\right)} \tag{11}$$

where l is the travel distance through the target, d is the vertical distance between source and top receiver, t and b are, respectively, the angles the top and bottom rays make with vertical in the overburden. By rewriting α in terms of frequency and Q and by replacing distances and velocities by the respective travel times, (11) becomes:

$$\left|\frac{R_2(\omega)}{R_1(\omega)}\right| = e^{-\left(\frac{\Delta t}{2Q_2}-\frac{\epsilon}{2Q_1}\right)\omega} \tag{12}$$

where Δt is the travel time through the target and the error term (ϵ) is defined as:

$$\epsilon = \frac{d}{c_1}\left(\frac{1}{\cos t}-\frac{1}{\cos b}\right) \tag{13}$$

which is the measure of the non-coincidence of the top and bottom reflection rays in the overburden for the model in Figure 1c. Taking the logarithm of (12) yields:

$$\ln\left|\frac{R_2(\omega)}{R_1(\omega)}\right| = -\left(\frac{\Delta t}{2Q_2}-\frac{\epsilon}{2Q_1}\right)\omega \tag{14}$$

which is a straight line equation with the same slope as equation (6) except for the error term $\frac{\epsilon}{2Q_1}$. Therefore, at non-zero offsets, the overburden contaminates the estimated target Q.

Equations (13) and (14) show that the significance of the error term in the slope depends on a number of factors. High error is introduced in Q estimation if the target is very thin relative to its depth. As the difference between the top and bottom reflection

ray trajectories in the overburden increases, more error is introduced to the estimation. Moreover, weakly attenuating target or highly attenuating overburden adversely affects the estimation accuracy. As a matter of fact, equation (14) predicts a threshold overburden Q below which estimated target Q is negative. To prevent such an effect at a given offset, the overburden Q should be:

$$Q_{\text{overburden}} > Q_{\text{target}} \frac{\epsilon}{\Delta t}.$$

Although this error analysis is carried out on transmitted waves, the conclusions still apply to reflected waves under the assumption that the overburden attenuation is homogeneous. Under this assumption, doubling the arrival times for the top and bottom waves will extend the results to estimating Q from reflected data. We can ignore reflectivity induced amplitude losses in this analysis because body wave dispersion is weak and thus reflectivity is almost frequency independent. Also, the reflectivity sequence in the propagation model is assumed to be white noise, making the ratio of the top and bottom reflectivities frequency independent. In this case, the reflectivity introduces an intercept to the spectral ratio, but the slope, which contains Q information, is not affected.

WATER TANK EXPERIMENT

Experimental Setup

In this experiment, three shot-gathers are acquired for three different materials, each submerged in a water tank. The source and receiver are positioned at the water surface as shown in Figure 2. Each target block is placed at a depth which separates the top and bottom reflections from the strong water bottom multiples. Table 1 lists the different materials used and their relevant properties, All the blocks have the same length and width (30 cm $\times$ 20 cm). Relative to the wavelength, all targets used in the experiment are considered thick.

The source used is a Panametrics (V303, 1MHz) transducer and the receiver is a B&K (8103) hydrophone. The source transducer is excited with a 100 Hz square function. Since the maximum recording time for each target is 5% of the period of the square function, the source signal is basically a step function. The data is low pass filtered and then recorded. The recorded source wavelet and its amplitude spectrum are shown in Figure 3. The source center frequency is around 250 kHz and the band width is rather narrow. However, obtaining constant Q values from such a spectrum was successful and quite robust. The source waveform has a long tail caused by internal reflections within the piezoelectric crystal in the transducer.

For each target, traces are recorded from 2 cm to 16 cm offset at a 2 cm traces interval. This offset distribution represents a range from 4°to 28°incidence angle at the level of the top of the target. The data sets collected for Lucite, rubber and Berea sandstone are shown in Figure 4. In the case of the sandstone, the bottom reflections are

	P-wave Velocity (m/s)	S-wave Velocity (m/s)	Density (kg/m^3)	Thickness (m)	Thickness (λ)	Actual Q
Water (overburden)	1500	0	1000	0.15	25	
Lucite	2700	1290	1180	0.1	9	50
Rubber	1600	800	1180	0.025	4	5–10
Berea sandstone	4400	1950	2080	0.1	5	20

Table 1:

locate the events. These events are then windowed and a cosine taper is applied at the beginning and end of the window to reduce edge effects in the frequency domain. The whole source waveform is used in Q estimation because both the main pulse and its tail pass through the target and should produce consistent Q values. Using the first cycle of the source wavelet artificially smoothes the spectral ratio. The estimates obtained by windowing either the whole waveform or the first cycle differ by no more than 20%. For each offset, the amplitude spectrum of the bottom reflection is normalized by the amplitude of the top reflection, and the slope term in equation (6) is used to estimate Q. The travel time through the target, needed to calculate Q, is estimated by a ray tracer which solves for the top and bottom ray geometries for both events to emerge at the offset of interest. However, estimating Q at this stage produces unrealistic and even negative values. The black curve in Figure 5 shows that the slope of the spectral ratio becomes positive at high frequencies and far offsets. This behavior implies that the top reflection is getting progressively weaker than the bottom reflection at far offsets. The radiation pattern of the source is believed to be the cause of this problem for two reasons. The first reason is that the inversion in the sign of the spectral ratio's slope occurs at higher frequencies than the source center frequency, where the radiation pattern is naturally narrower than at low frequencies. The second reason is that due to the velocity increase at the top of the target, the take off angle of the top reflection ray is larger than the take off angle of the bottom reflection ray which weakens the amplitude spectrum of the top reflection relative to the bottom reflection at large offsets. Due to this effect, the top and bottom amplitude spectra have to be corrected for the source radiation pattern before attempting to estimate Q.

Source Radiation Pattern Correction

The amplitude spectra of the reflections are corrected for the source radiation empirically. To do so, a new data set is acquired in which the source is positioned at the water surface and the receiver is placed at the depth of the top of the target. The receiver is then moved from directly under the source to 19 cm offset with the direct arrival being recorded at 1 cm trace interval, see Figure 6. The direct arrivals sample the source radiation pattern from 0°to 52°at an increment of 2°. After correcting for divergence,

radiation pattern before attempting to estimate Q.

Source Radiation Pattern Correction

The amplitude spectra of the reflections are corrected for the source radiation empirically. To do so, a new data set is acquired in which the source is positioned at the water surface and the receiver is placed at the depth of the top of the target. The receiver is then moved from directly under the source to 19 cm offset with the direct arrival being recorded at 1 cm trace interval, see Figure 6. The direct arrivals sample the source radiation pattern from 0°to 52°at an increment of 2°. After correcting for divergence, the amplitude spectra for each direct arrival is computed and the amplitude drop for each source frequency component as a function of take off angle is normalized by the amplitude at 0°. Figure 7 shows both raw and smoothed versions of the normalized amplitude drop at 120 kHz, 270 kHz and 390 kHz. It is obvious from the figure that the amplitude loss is most significant at high frequencies. The smoothed curves are used to build the radiation pattern of the source at all of the significant source frequencies. Figure 8 shows the computed radiation curves at selected frequencies. The correction of the amplitude spectrum of an event will start with calculating the take off angle from the source. This angle is used to find the associated normalized source amplitude for each frequency, then the amplitude spectrum of the event is divided by the normalized source amplitude. Applying this correction significantly improves Q estimates, especially for far offsets. Figure 5 shows the difference between the spectral ratios before and after the radiation correction.

Estimated Q Values

The final Q estimates for the different targets as a function of offset are shown in Figure 9a. According to Toksöz *et al.* (1979), the actual values for Lucite and Berea Sandstone are 50 and 20, respectively. Rubber is known to be a highly attenuating material with Q between 5 and 10.

The estimated Q values for Lucite ranges from 40 at 2 cm offset to 45 at 16 cm offset. For the sandstone, the values range from 22 to 32. For both materials, Q values increase with offset. Although there is no firm reference estimate for rubber, the estimated Q values show the same behavior with offset as the other two targets with Q increasing from 18 to 20. The increase in the Q value with offset relative to the near offset estimate is most pronounced in the sandstone and least noticeable in the rubber Q estimates. Figure 9b shows the behavior of Q estimates with offset dur to overburden attenuation as equation (14) predicts. To compute each curve in Figure 9b, the slope term in equation (14) is evaluated for each target using the actual target Q, a Q of 150 for water and the ray path lengths for the top and bottom reflections calculated by ray tracing. Using this slope, Q is evaluated at each offset which shows the ideal Q deviation from the true value due to overburden effects.

Interval Attenuation Estimation

With Q values ranging from 50 to 54, Lucite shows the most pronounced drift from the actual Q among the other targets. This behavior is supported by the fact that Lucite is the least attenuating target and that the difference between the top and bottom reflection ray paths in the water is considerable. The Q values for the Berea Sandstone shows a drift from 20 to 23 with offset. Although the ray non-coincidence in water for the sandstone is more significant than in the case of Lucite, the high attenuation of the sandstone reduces the drift from the near offset Q value. The low P-wave velocity and the high attenuation of rubber lead to the least increase in Q values with offset.

The experimental Q estimates shown in Figure 9a contain other sources of error in addition to overburden induced error. These errors arise from noise in the data, amplitude spectrum estimation and spectral ratio slope estimation. However, for the case of Lucite and rubber Q estimates, the behavior of increasing Q value with offset is noticeable. The amount of the drift from the near offset estimate is very close to the ideal computed drift in Figure 9b. The deviation from near offset value in the case of the sandstone is more than anticipated by theoretical error analysis. This mismatch is attributed to difficulties in calculating the amplitude spectrum of far offset sandstone bottom reflections due to the low transmission coefficient at the water-sandstone interface.

CONCLUSIONS

In this study, the spectral ratio method is applied to ultrasonic lab reflection data to estimate the Q value of different blocks of target material submerged in a water tank. The different materials used are Lucite, rubber and Berea sandstone. Theoretical error analysis shows that the effects of an attenuating overburden on the estimated target Q are eliminated by applying the spectral ratio method to zero-offset reflections. However, at other offsets, the overburden will contaminate the Q estimate. The derived theoretical error term shows that the error in estimated Q due to the overburden is directly proportional to the ratio of the target depth to its thickness, the target Q value, the attenuation of the overburden and the difference in top and bottom reflection ray path lengths in the overburden. Additionally, the difference in the ray lengths is controlled by the velocity distribution in and above the target.

For Lucite, with actual Q of 50, the estimated Q values range from 40 at the near offset to 45 at the far offset. For the sandstone, with reference Q of about 20, the estimates range from 22 at the near offset to 32 at the far offset. The Rubber Q values run from 17 to 20. The estimates for all the targets show an increase in Q with offset. This behavior with offset is believed to be caused by overburden attenuation as equation (14) predicts. The increase in estimated Q with offset for the Lucite and rubber targets agrees with that predicted by theory. The deviation from the near offset estimate for the sandstone target exceeds that predicted by theory. This discrepancy is attributed to noise contaminating the bottom sandstone reflections due to the small transmission coefficient at the top of the target.

ACKNOWLEDGMENTS

Hafiz Alshammery and this work are supported by Saudi ARAMCO. This work was also supported by the Borehole Acoustics and Logging/Reservoir Delineation Consortia at the Massachusetts Institute of Technology. We would like to thank Dr. Zhenya Zhu at MIT's Earth Resources Laboratory for lab assistance.

REFERENCES

Akbar, N., Dvorkin, J. and Nur, A., 1993, Relating P-wave attenuation to permeability, *Geophysics, 58,* 20–29.

Akbar, N., Mavko, G., Nur, A., and Dvorkin, J., 1994, Seismic signature of reservoir transport properties and pore fluid distribution, *Geophysics, 59,* 1222–1236.

Baranowski, J., 1980, Determination of seismic attenuation using observed phase shift in sedimentary rocks, M.S. thesis, MIT.

Bickel, S. and Natarajan, R., 1985, Plane-wave Q deconvolution, *Geophysics, 50,* 1426–1439.

Dasgupta, R. and Clark, R., 1994, Successful estimation of Q from surface seismic data: methodology and case studies, *64 Internat. Mtg., Soc. Expl. Geophys., Expanded Abstracts,* 1602–1605.

Dvorkin, J., Nolen-Hoeksema, R., and Nur, A., 1994, The squirt flow mechanism, macroscopic description, *Geophysics, 59,* 428–438.

Jacobson, R., 1987, An investigation into the fundamental relationships between attenuation, phase dispersion, and frequency using seismic refraction profiles over sedimentary structures, *Geophysics, 52,* 72–87.

Liao Q. and McMechan, G., 1997, Tomographic imaging of velocity and Q, with application to crosswell seismic data from the Gypsy Pilot Site, Oklahoma, *Geophysics, 62,* 1804–1811.

Shatilo, A., 1994, One property of attenuation and estimation of seismic attenuation from field data, *64 Internat. Mtg., Soc. Expl. Geophys., Expanded Abstracts,* 1599–1601.

Stainsby, S. and Worthington, M., 1985, Q estimation from vertical seismic profile data and anomalous variations in the central North Sea, *Geophysics, 50,* 615–626.

Toksöz, M.N. and Johnston, D. (eds.), 1981, *Seismic Wave Attenuation,* SEG.

Toksöz, M.N., Johnston, D., and Timur, A., 1979, Attenuation of seismic waves in dry and saturated rocks, I. Laboratory measurements, *Geophysics, 44,* 681–690.

White, R., 1992, The accuracy of estimating Q from seismic data, *Geophysics, 57,* 1508–1511.

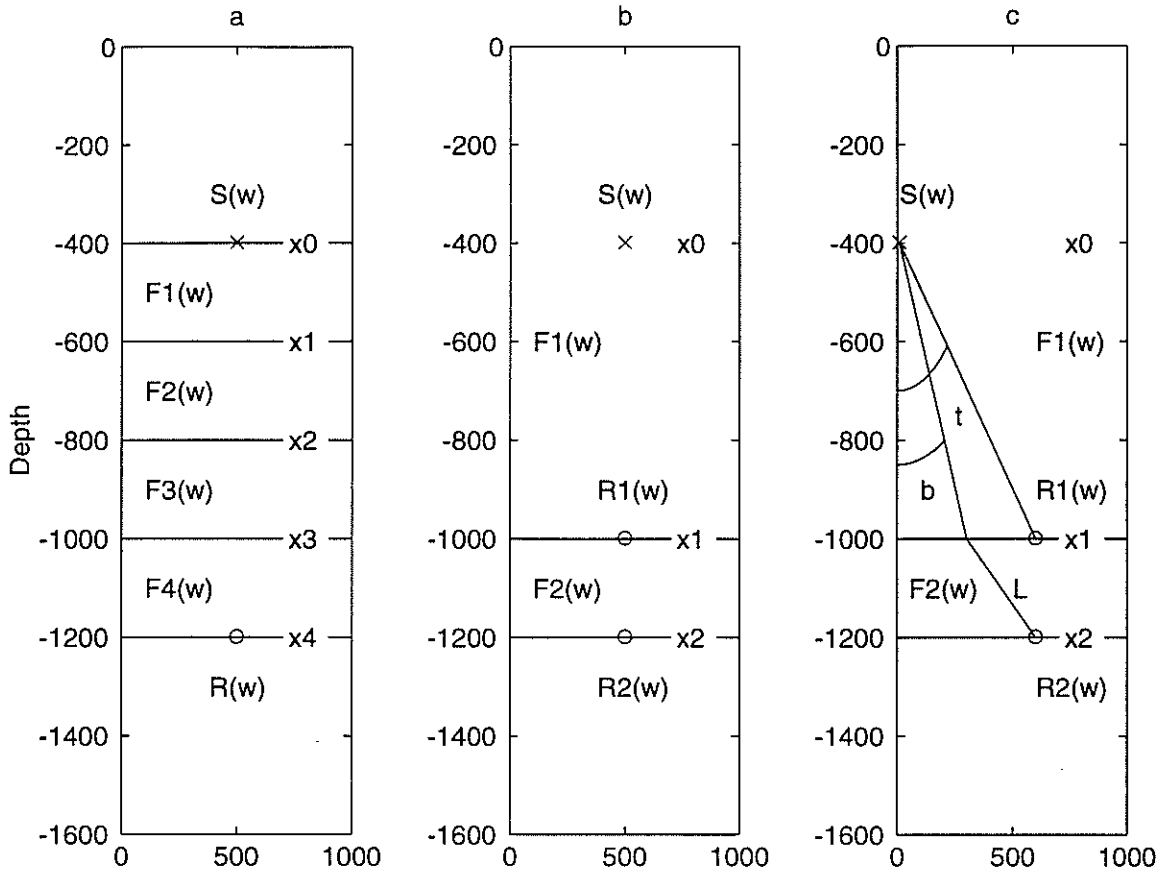

Figure 1: The different earth models used in error analysis. (a) is the generalized model. (b) is the simplified model for zero-offset analysis. (c) is the non-zero offset model. Angles t and b are the take off angles of the waves received at the top and bottom of the target. The travel distance in the target is L.

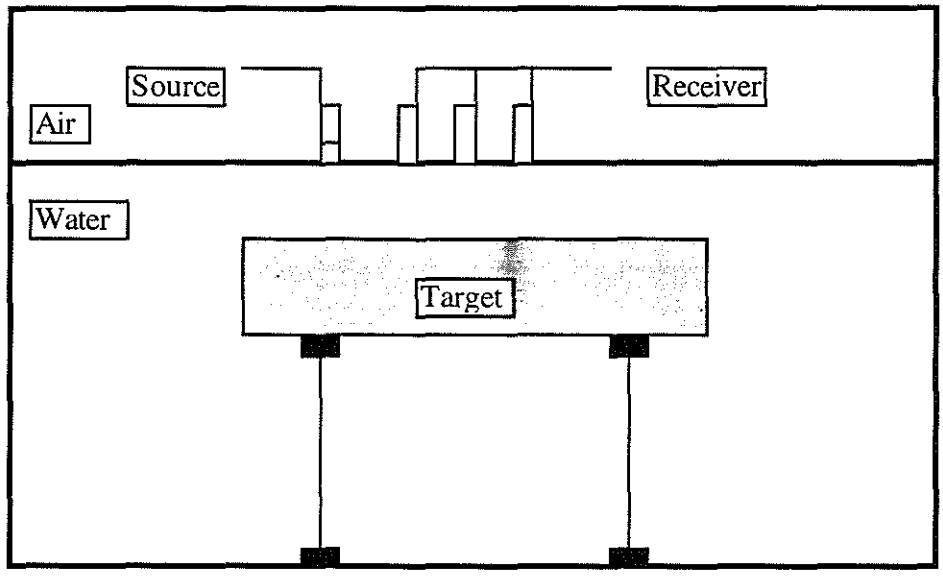

Figure 2: Water tank experiment setup.

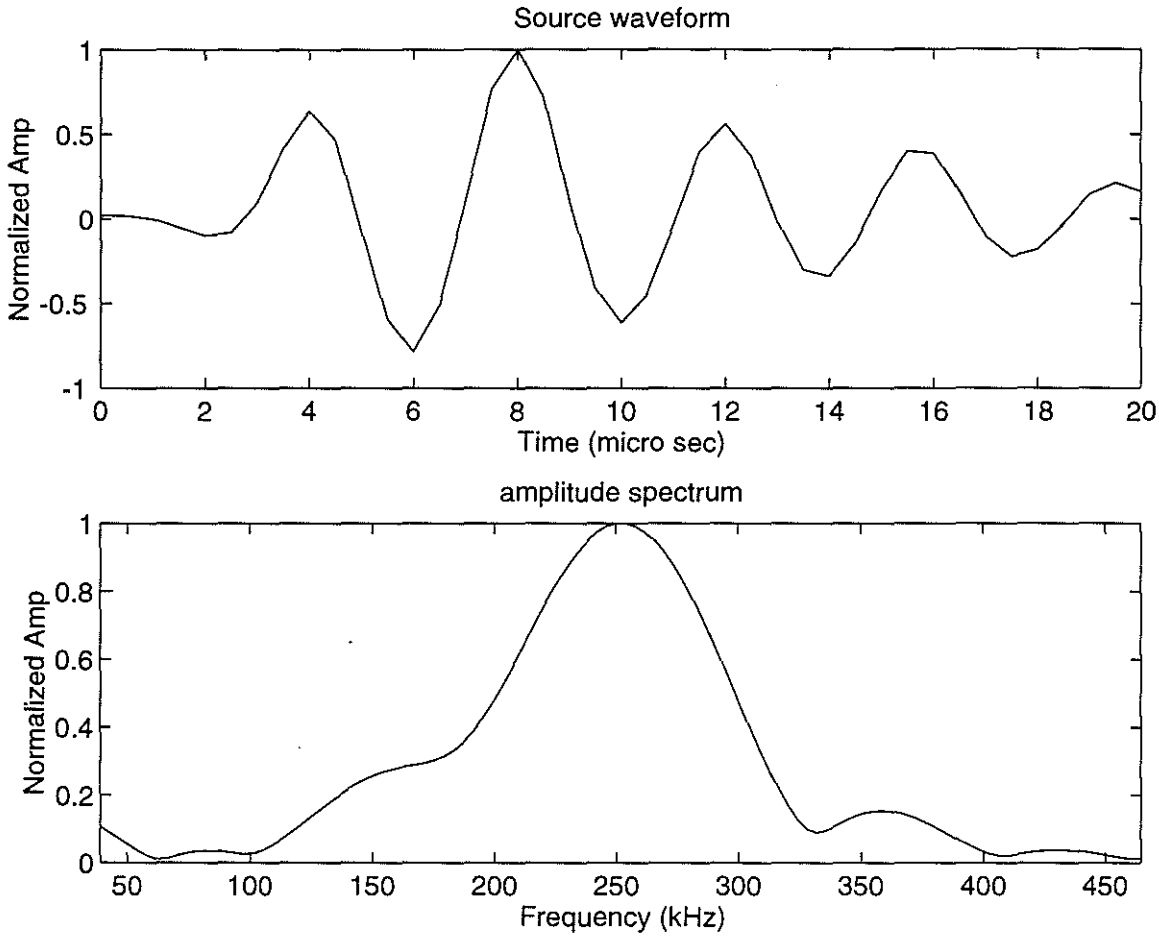

Figure 3: The basic source wavelet and its amplitude spectrum.

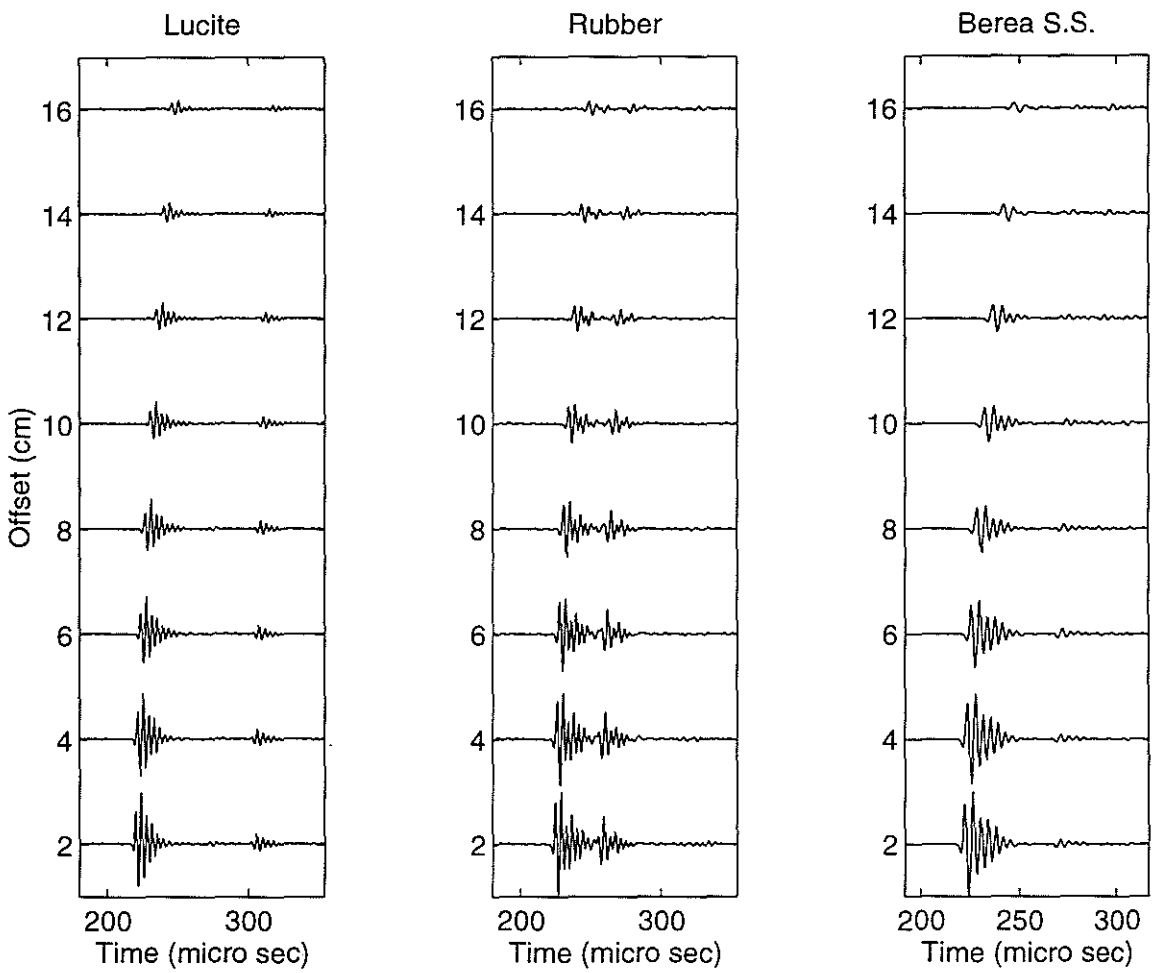

Figure 4: Shot gathers recorded for Lucite, rubber and Berea sandstone targets using the setup shown in Figure 2.

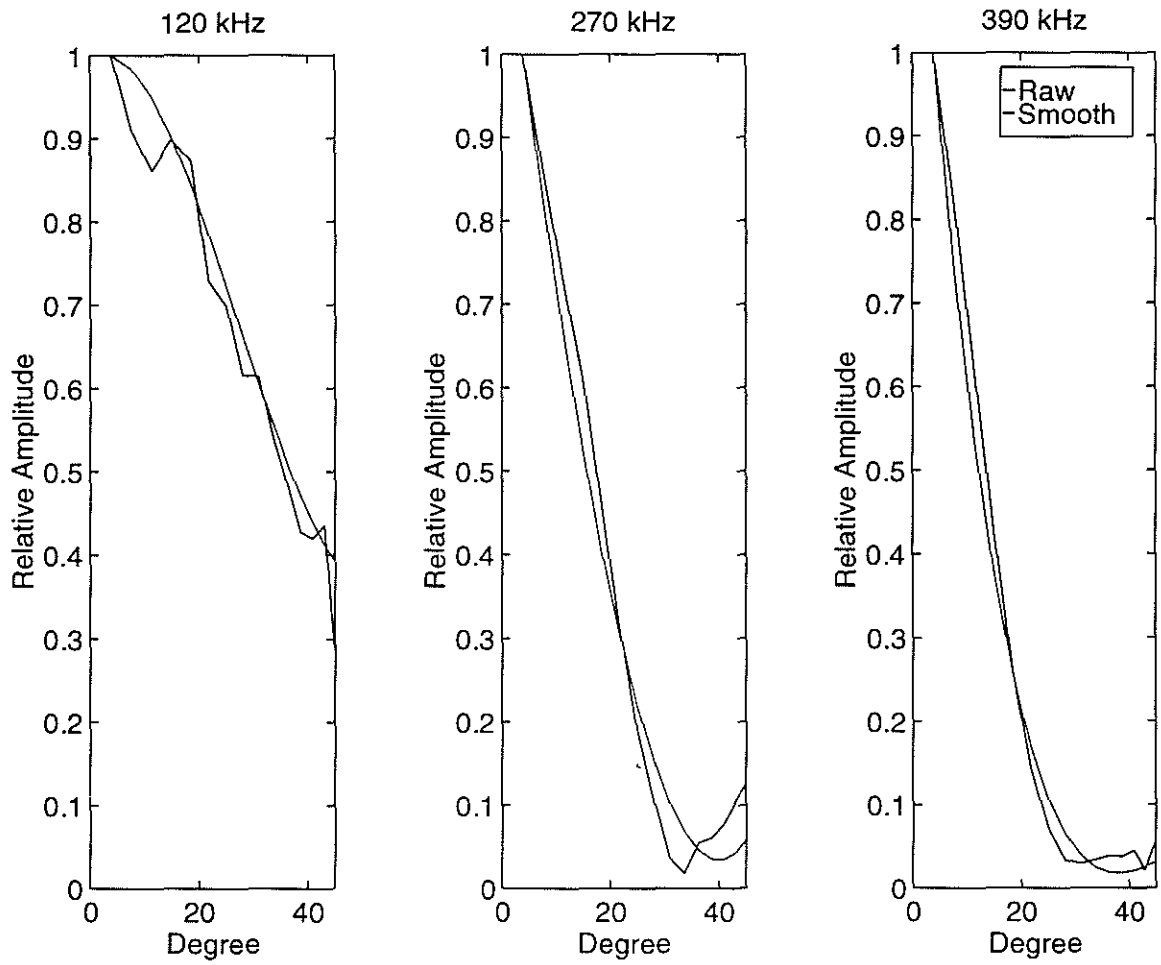

Figure 7: The amplitude drop as a function of take off angle for selected source frequencies.

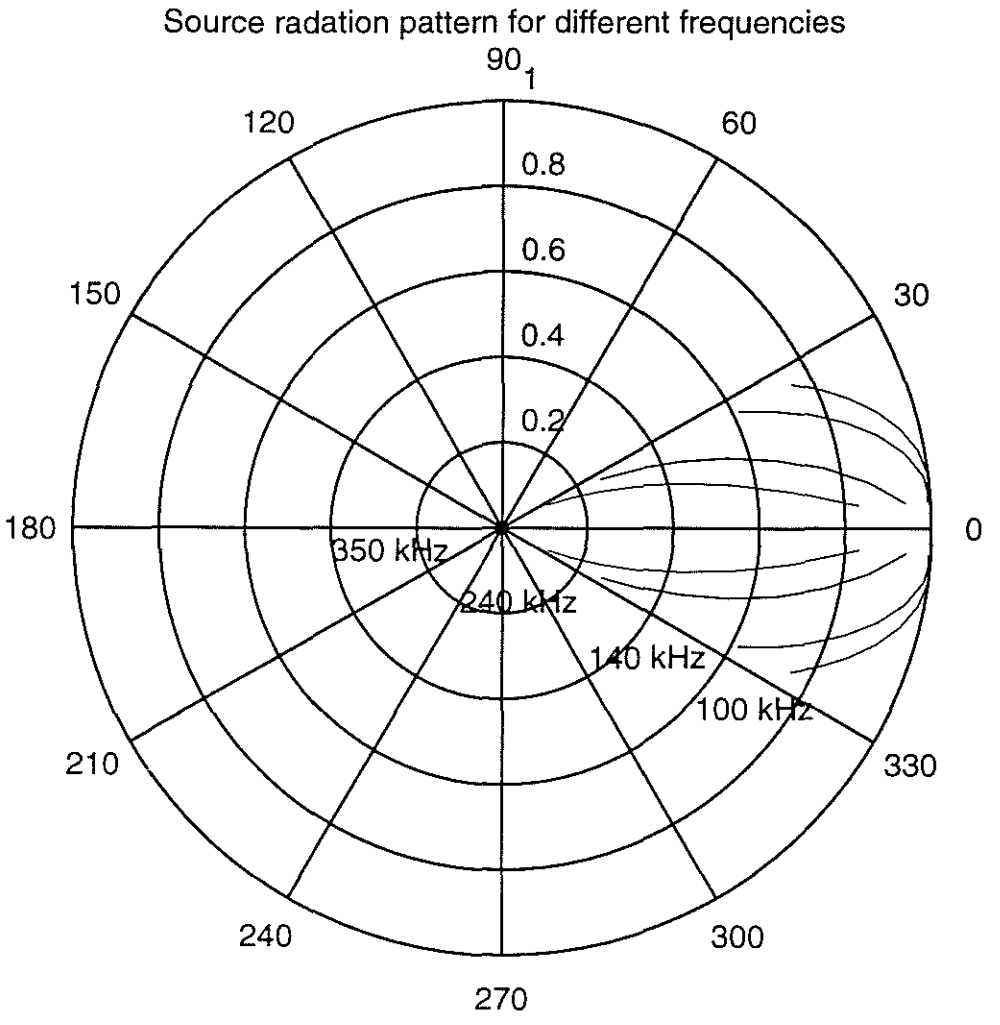

Figure 8: Radiation pattern derived from curves in Figure 7. These patterns are used to correct the data for source directivity.

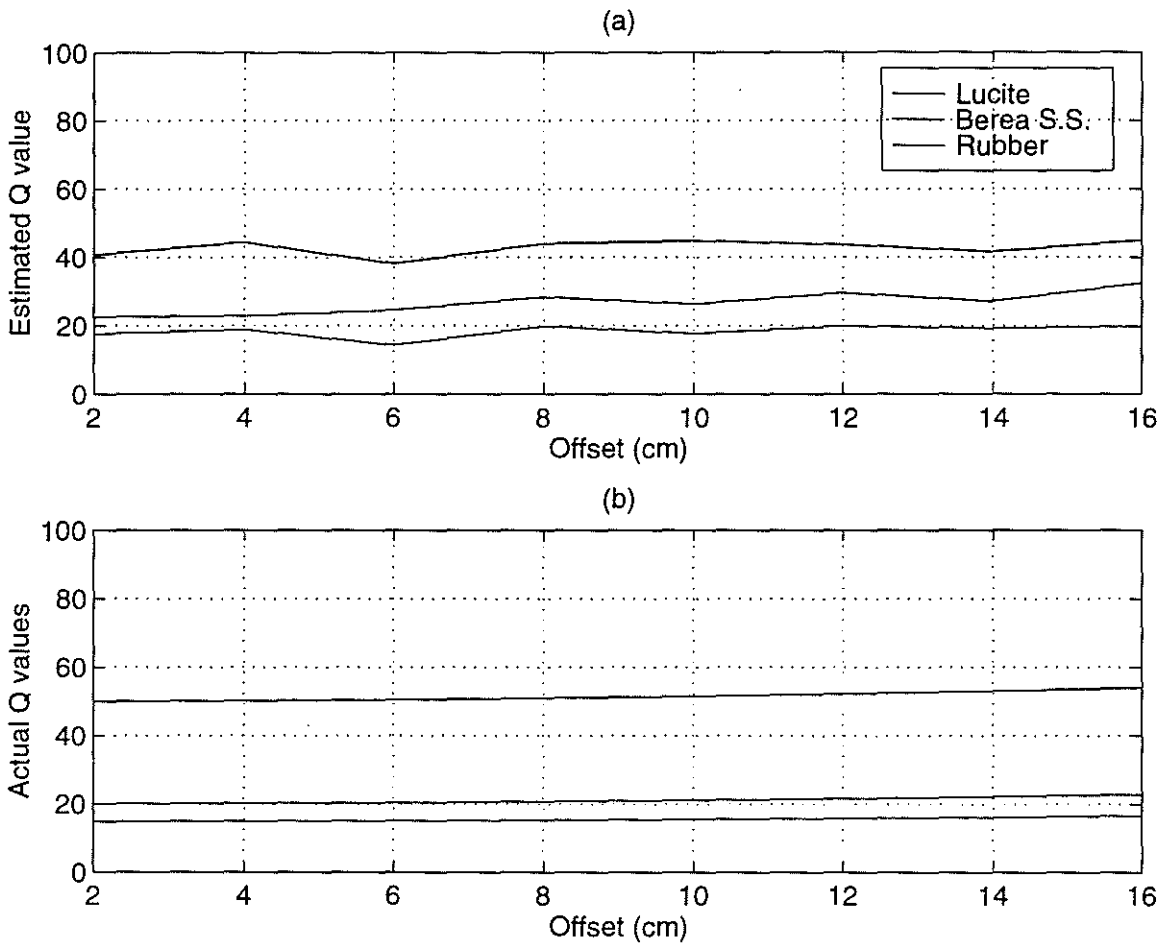

Figure 9: (a) the experimentally computed Q values for the different targets. (b) The theoretical drift from actual Q value due to overburden effects only.